Supplementary information for

Role of Aluminum in Controlling Defect Formation and Polytypism in Silicon Carbide via Thermal Synthesis

Author list: Sarah Morais Bezerra[1,2], Sándor Kollarics[1,3,4], Luisa Souza Almeida[5], Gábor Bortel[1], Nikoletta Jegenyes[1], Bence Gábor Márkus[6,1], Ferenc Simon[1,4,6], Adam Gali[1,7,8*] and David Beke[1,9,*]

X-ray Diffraction Data

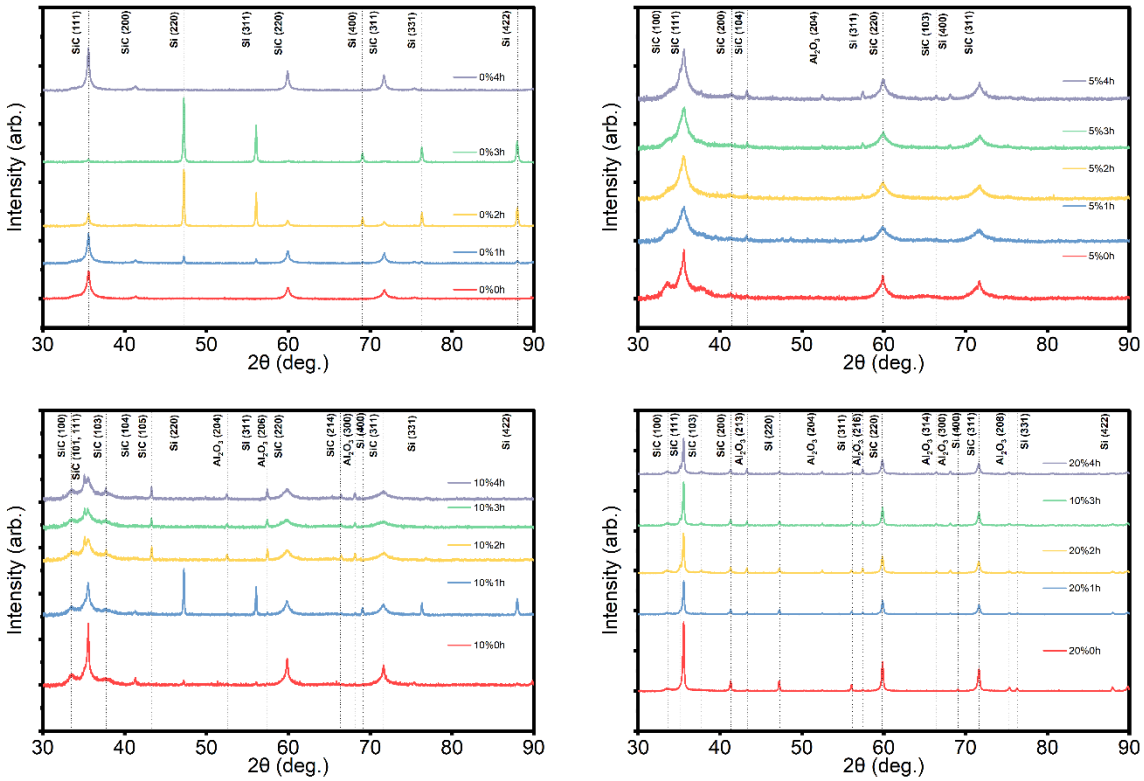

Figure S1. X-ray diffractograms after 0-4h milling times for samples a) 0%, b)5%, c)10% and d) 20% Al added to the precursor mixture.

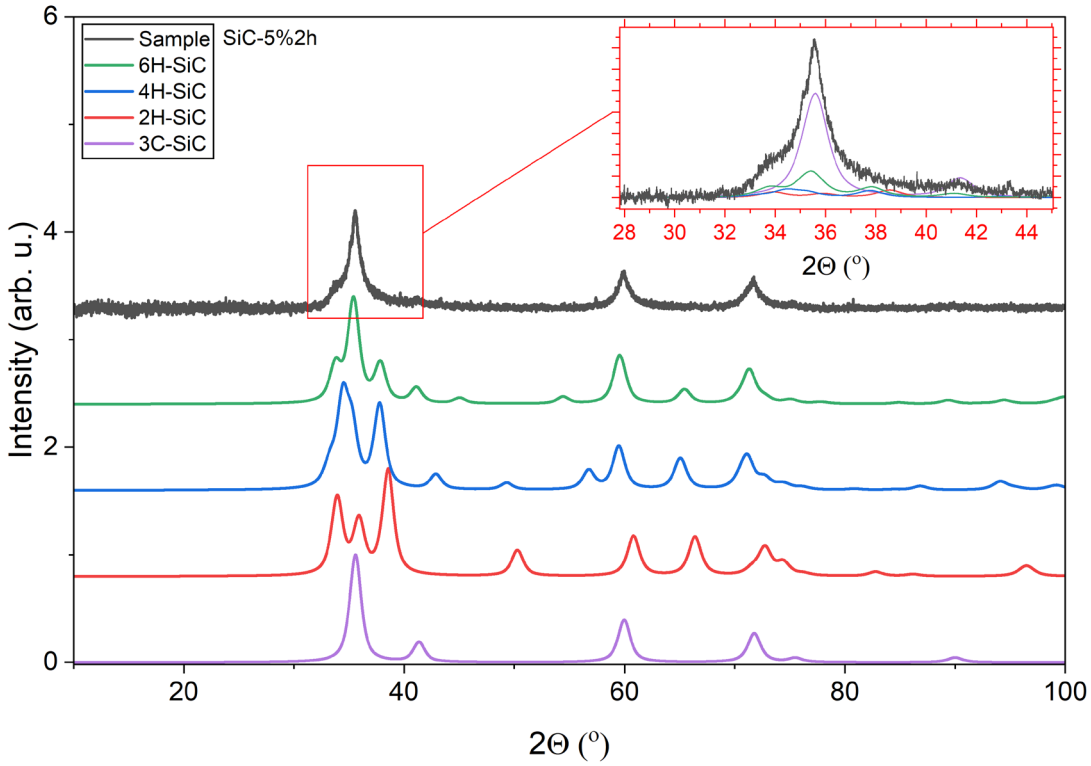

Figure S2. X-ray diffractogram for 5%Al-2h sample with the Rietveld fitting showing each polytype used for Rietveld refinement.

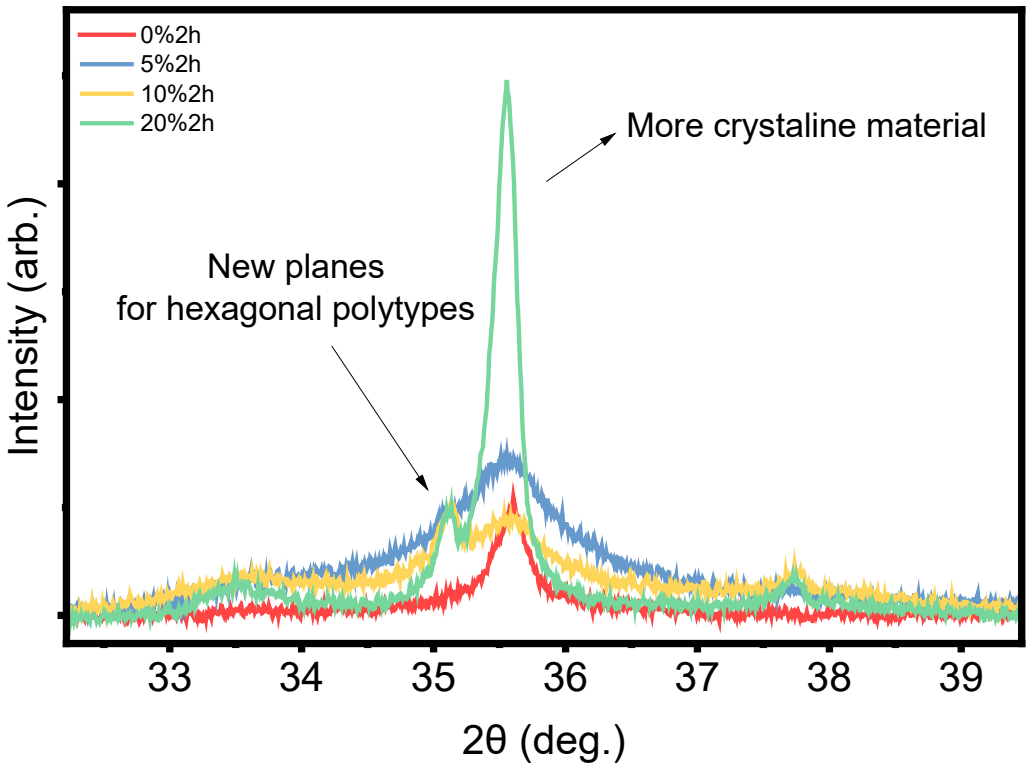

Figure S3. XRD comparison after reaction and the effect of Al on the peaks of the samples.

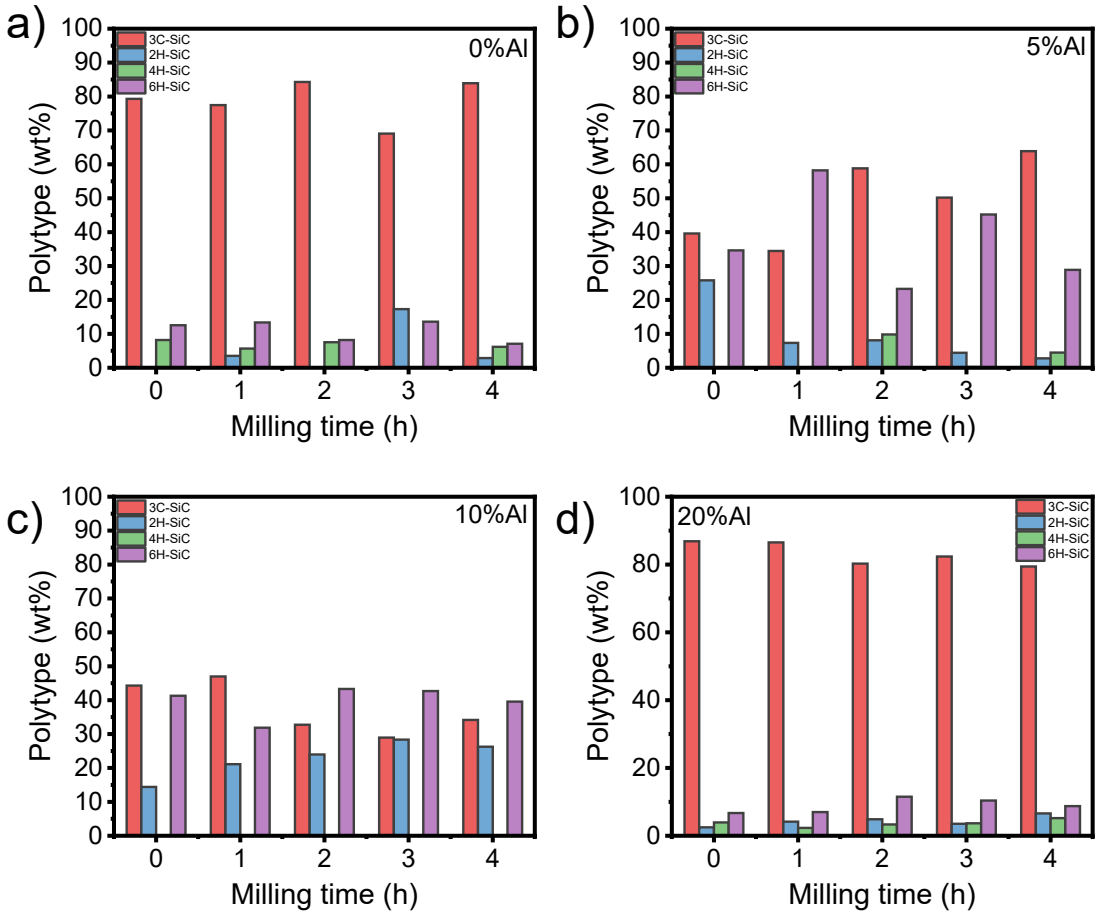

Figure S4. Result from the Rietveld fitting (polytype composition) after 0-4h milling times for samples a) 0%, b)5%, c)10% and d) 20% Al added to the precursor mixture.

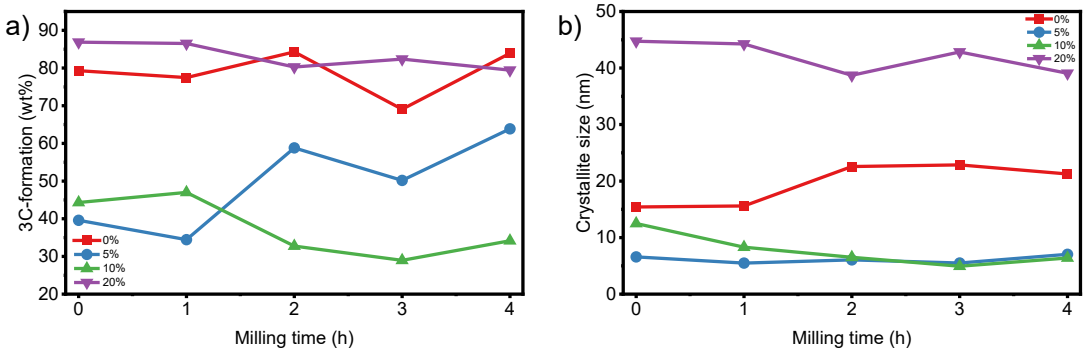

Figure S5. Cubic phase content (a) and crystallite size (b) as functions of milling time. These data are identical to those presented in Fig. 3 of the main text, where they were depicted as functions of Al concentration in the precursor.

Raman Data

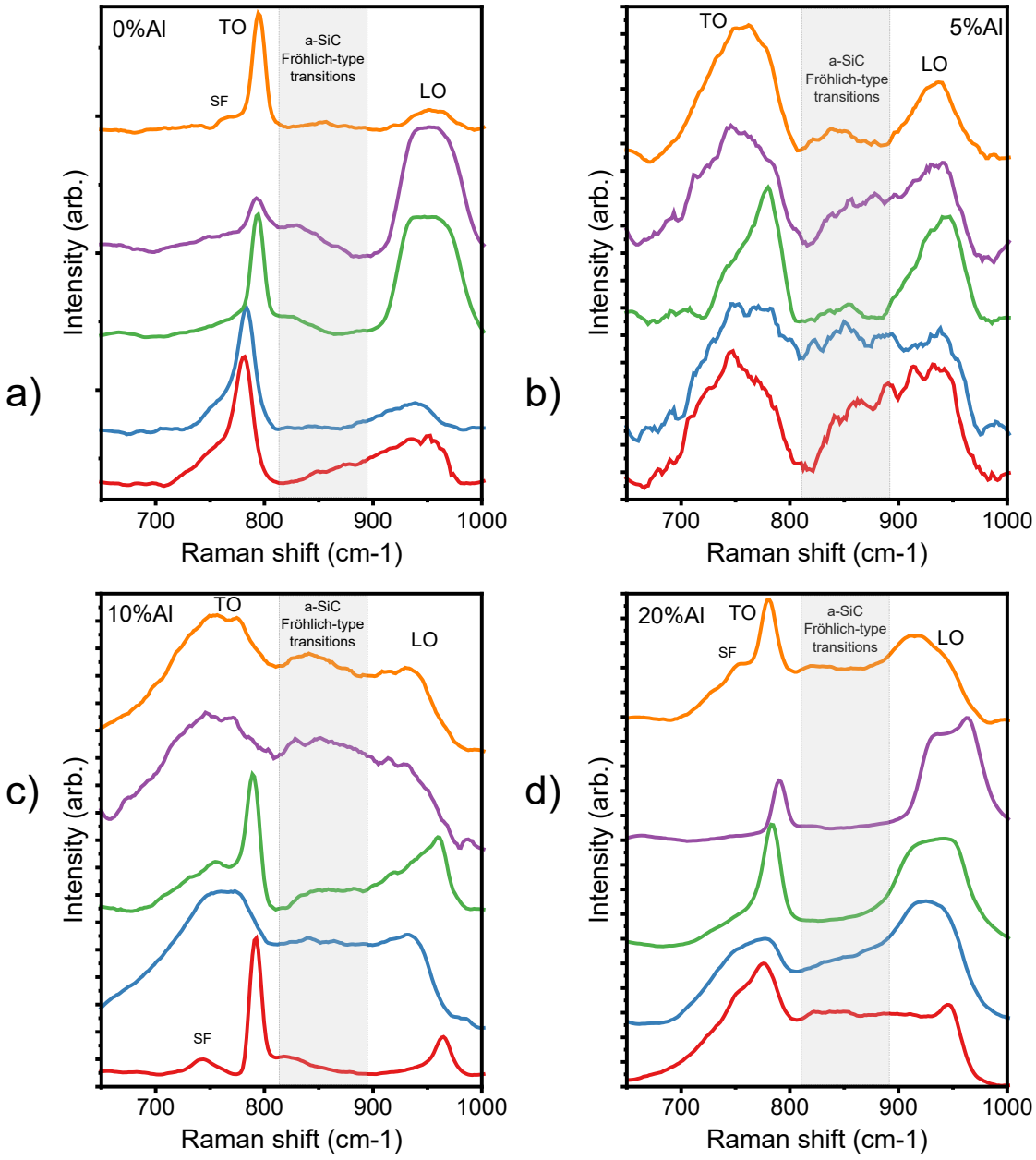

Figure S6. Raman spectra of the samples after 0-4h milling times for samples a) 0%, b)5%, c)10% and d) 20% Al added to the precursor mixture.

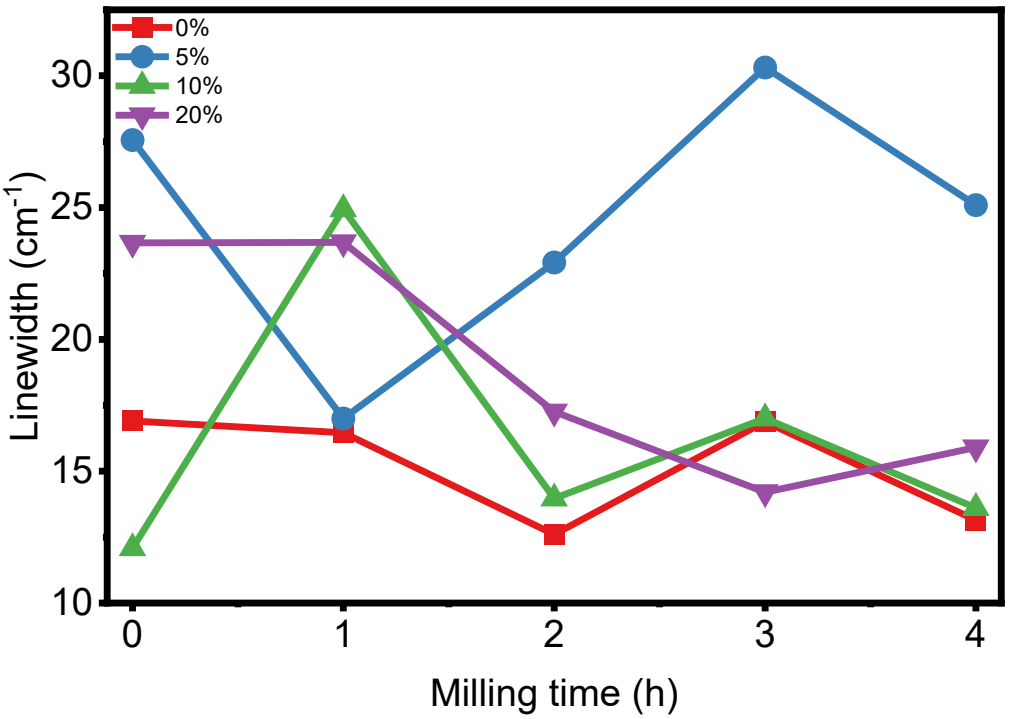

Figure S7. Linewidth of TO peaks after fitting with a Voigt function, that correlates with SF concentration[70,72] as functions of milling time. These data are identical to those presented in Fig. 4 of the main text, where they were depicted as functions of Al concentration in the precursor.

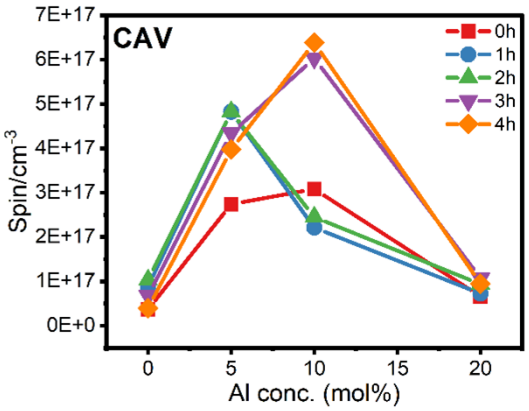

Figure S8 Area for the Raman peak around 720-730 cm^{-1} This area has been associated with the presence of CAV in SiC

EPR Data

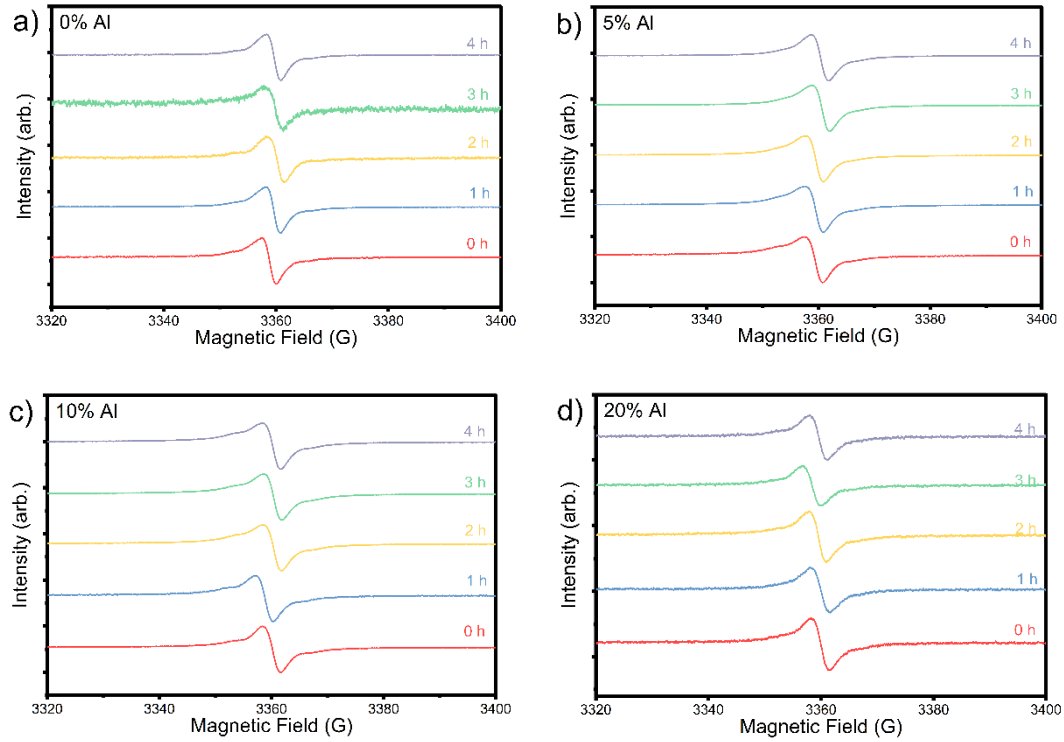

Figure S9. EPR spectra after 0-4h milling times for samples a) 0%, b)5%, c)10% and d) 20% Al added to the precursor mixture**.**

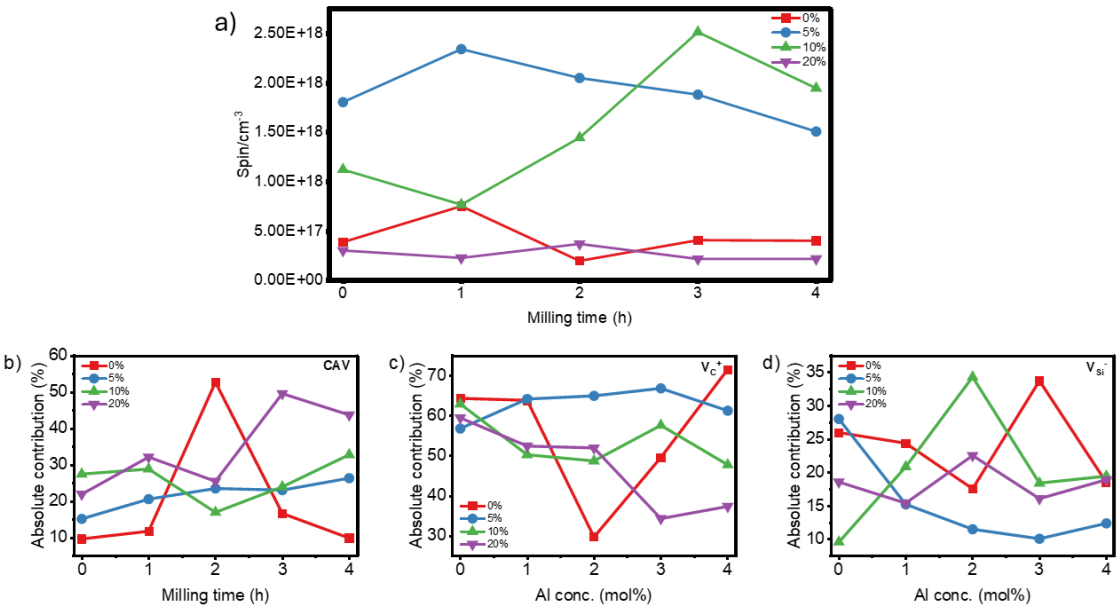

Figure S10. a) Calculated defect concentration as a function of Al concentration in the precursor for various milling times. The contribution of the three vacancies, b) carbon antisite vacancy pair (CAV), c) carbon vacancy (V_C^+), and d) silicon vacancy (V_{Si}^-), which were used to simulate the experimental data. These data are identical to those presented in Fig. 5 of the main text, where they were depicted as functions of Al concentration in the precursor.

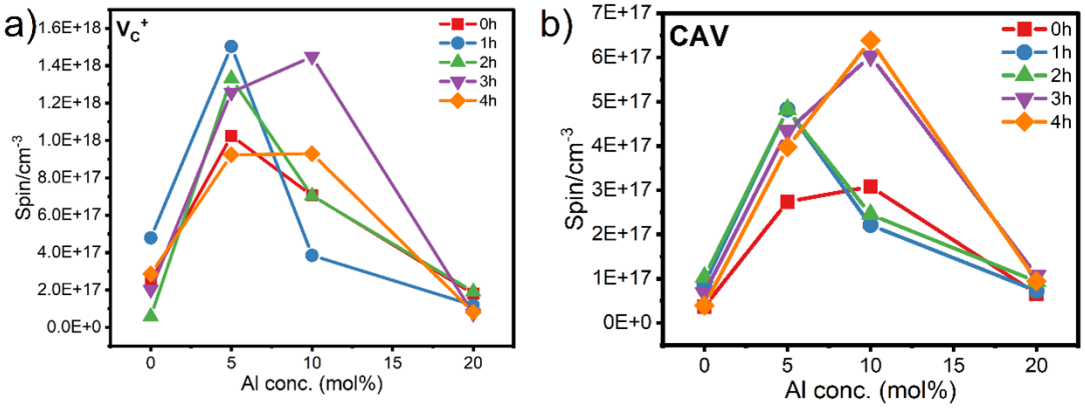

Figure S11. Calculated defect concentration as a function of Al concentration in the precursor for various milling times. The spin concentratin a) carbon vacancy (V_C^+) and b) carbon antisite vacancy pair (CAV), silicon vacancy (V_{Si}^-) can be found in the main text.

Photoluminescence Measurement Data

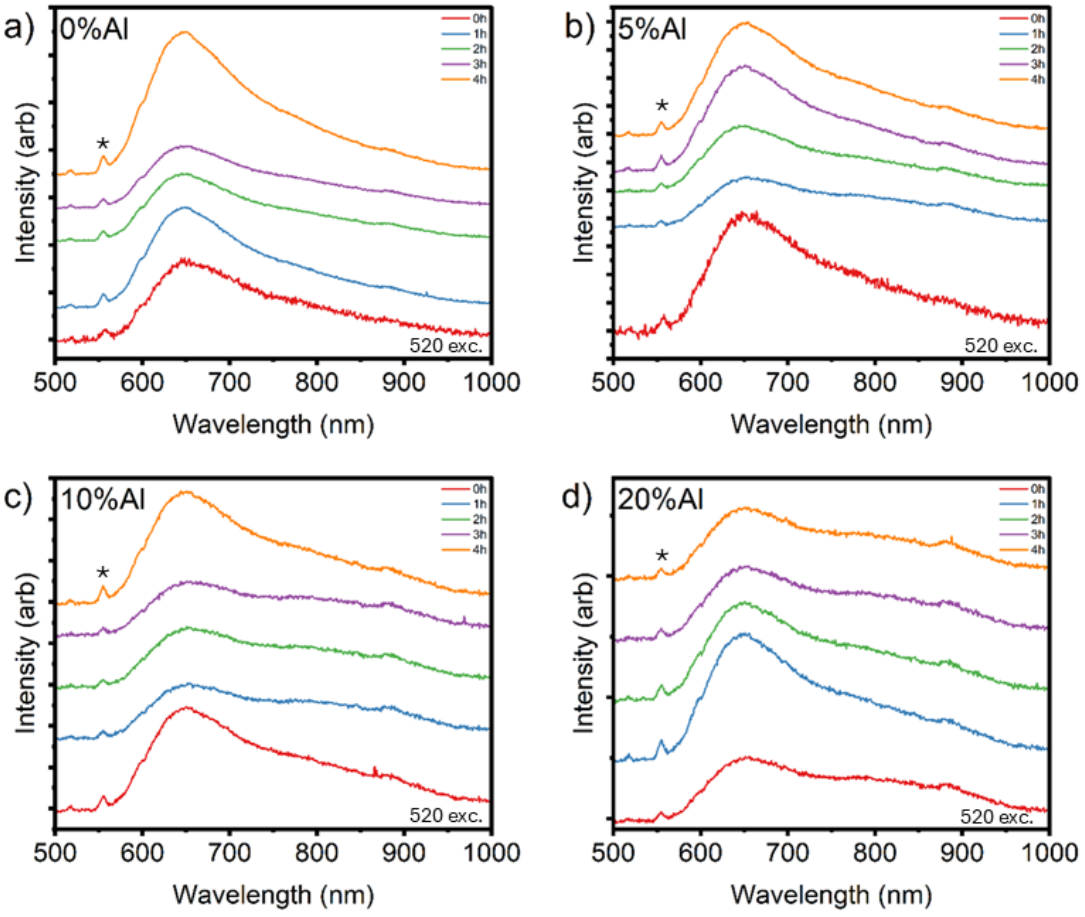

Figure S12. PL measurements were acquired using a 520 nm excitation laser after 0-4h milling times for samples a) 0%, b)5%, c)10% and d) 20% Al added to the precursor mixture The asterisk (*) denotes an artifact originating from the sample holder.

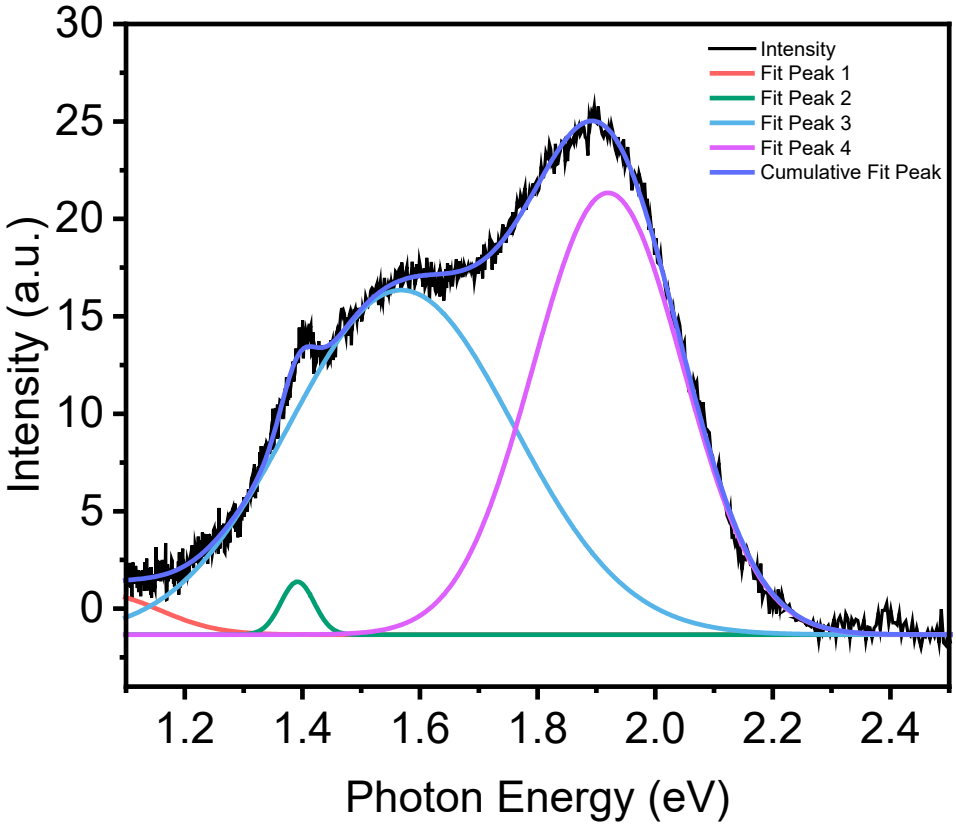

Figure S13. Example of a fitting procedure used to extract the peak values from photoluminescence (PL) spectra.

Statistical Calculations

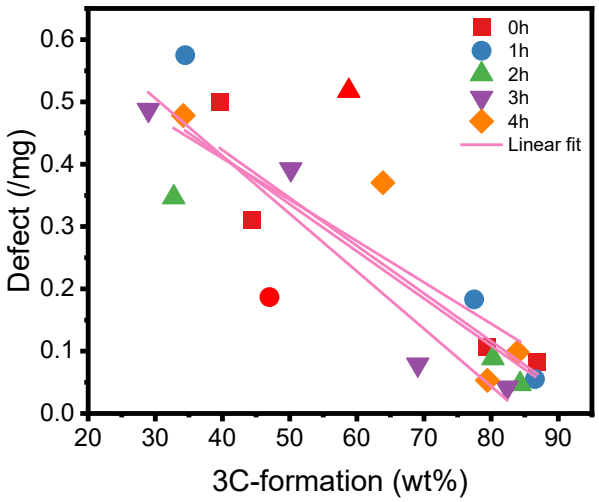

Figure S14 Linear regression model used to calculate the values of Pearsons *r* values of -0.94, -0.99, -0.99, -0.96, and -0.92 for time intervals of 0 h, 1 h, 2 h, 3 h, and 4 h, respectively.

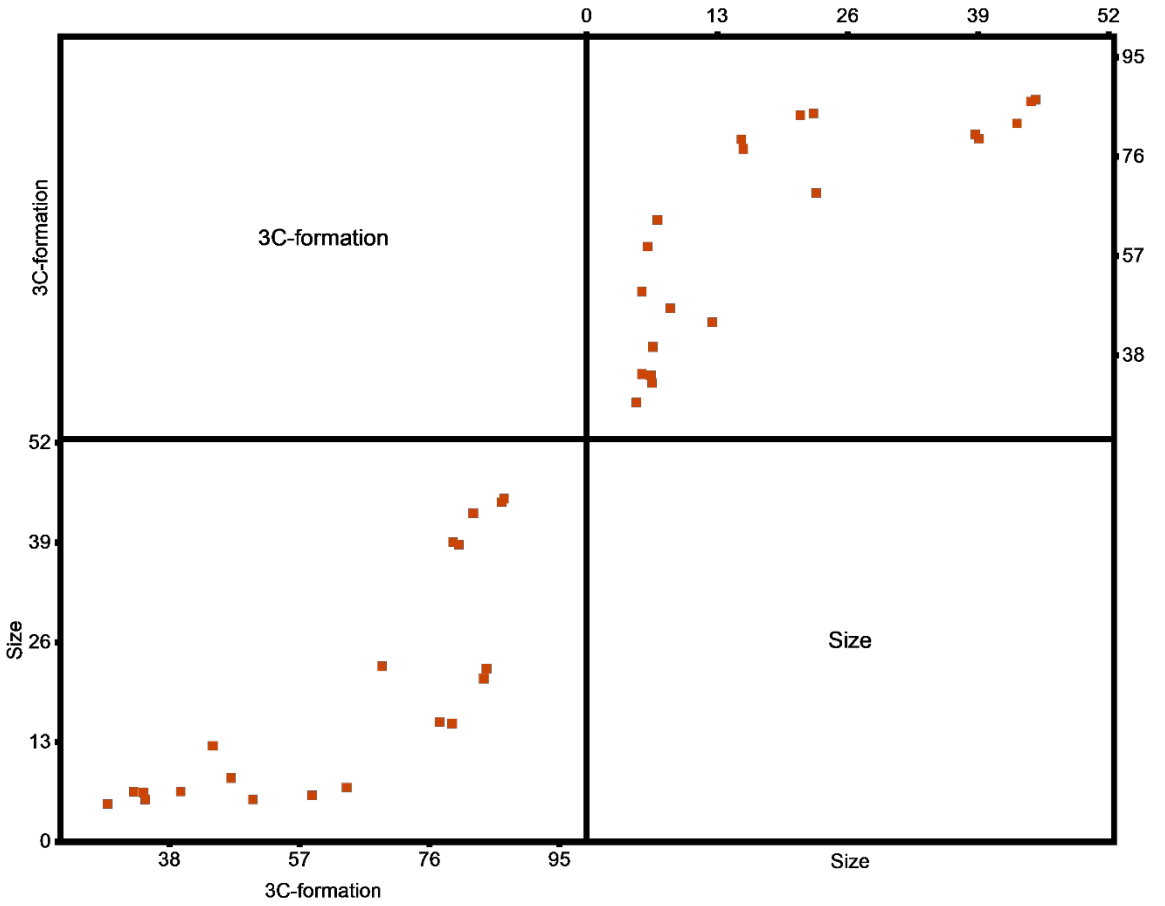
0
13
26
39
52
95
76
57
38
3C-formation
3C-formation
52
39
26
13
0
Size
Size
38
57
76
95
3C-formation
Size

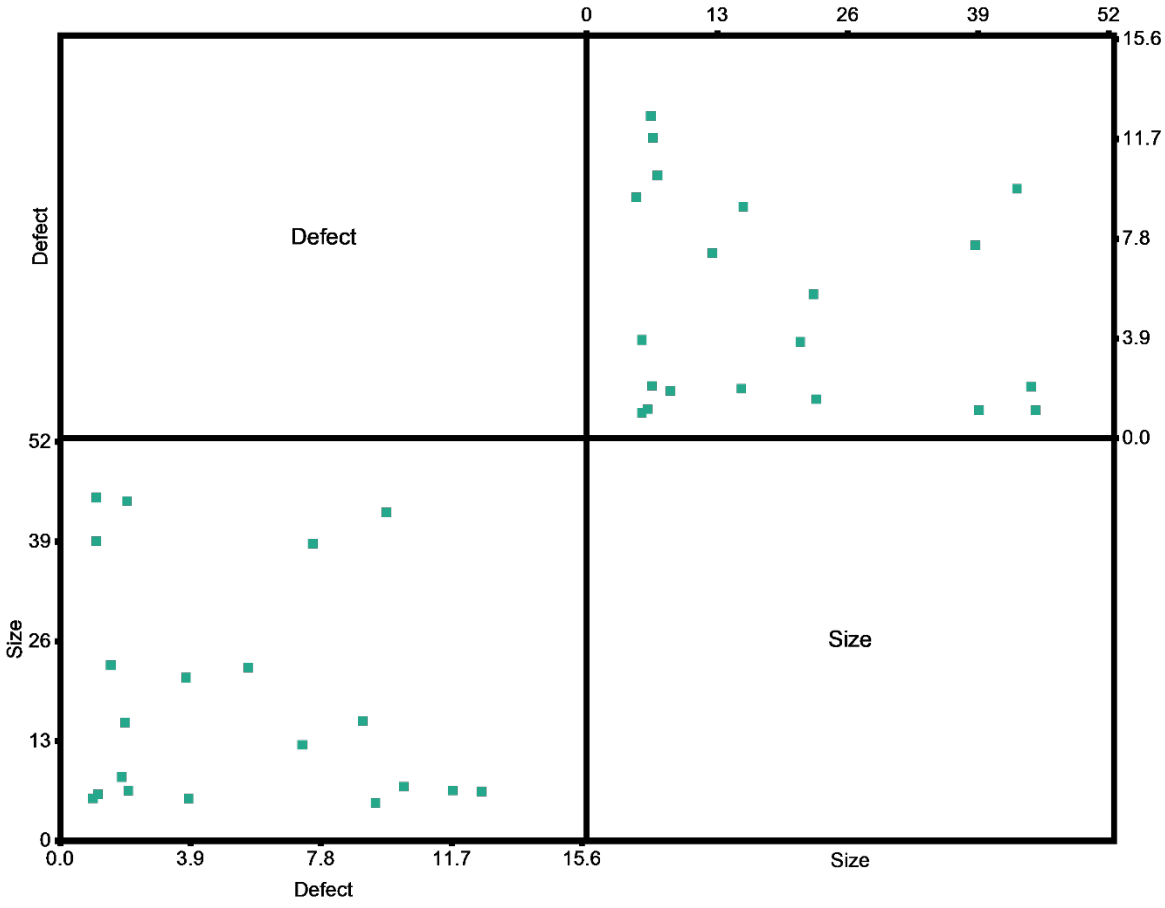
0
13
26
39
52
15.6
11.7
7.8
3.9
0.0
Defect
Defect
52
39
26
13
0
Size
Size
0.0
3.9
7.8
11.7
15.6
Defect
Size

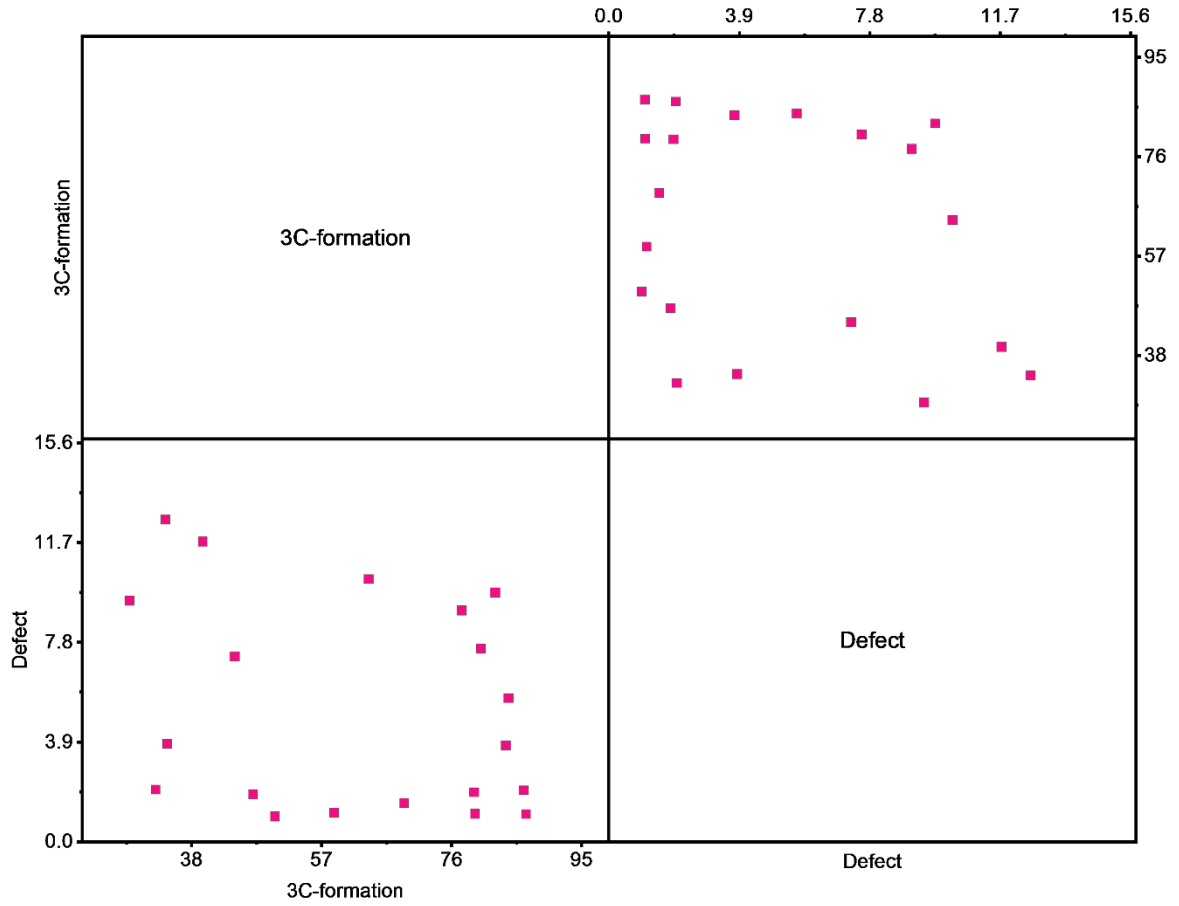

Figure S15. Spearman scatter matrix for b) size vs. 3C-formation (r_s = 0.87, p-value < 0.0001), c) size vs. defect (r_s = -0.20, p-value = 0.38) and d) 3C-formation vs. defect (r_s = -0.26, p-value = 0.25).

Table S1. Spearman's correlation results for 3C-formation vs. size

Sample	**r_s**	**p-value**
0h	1	< 0.0001
1h	1	< 0.0001
2h	0.6	0.4
3h	1	< 0.0001
4h	0.8	0.2

Table S2. Spearman's correlation results for defect vs. size.

Sample	**r_s**	**p-value**
0h	-1	< 0.0001
1h	0	1
2h	1	< 0.0001
3h	0.4	0.6
4h	-1	< 0.0001

Table S3. Spearman's correlation results for defect vs. 3C-formation.

Sample	r_s	p-value
0h	-1	< 0.0001
1h	0	1
2h	0.6	0.4
3h	0.4	0.6
4h	-0.8	0.2

Table S4. Pearsons' r results for size vs defects.

Sample	r	R^2
0h	-0.31	0.09
1h	-0.15	0.02
2h	0.31	0.10
3h	-0.63	0.4
4h	0.018	0.00003

Table S5. Pearsons' r results for size vs 3C-formation.

Sample	r	R^2
0h	0.15	0.02
1h	0.42	0.18
2h	-0.85	0.58
3h	0.70	0.50
4h	-0.11	0.012

Table S6. Raman PCA results.

component	eigenvalue	explained variance %	cumulative variance %
'PC1'	'7.4363'	'47.0743'	'47.0743'
'PC2'	'4.9107'	'31.0866'	'78.1609'
'PC3'	'1.3121'	'8.3062'	'86.4671'

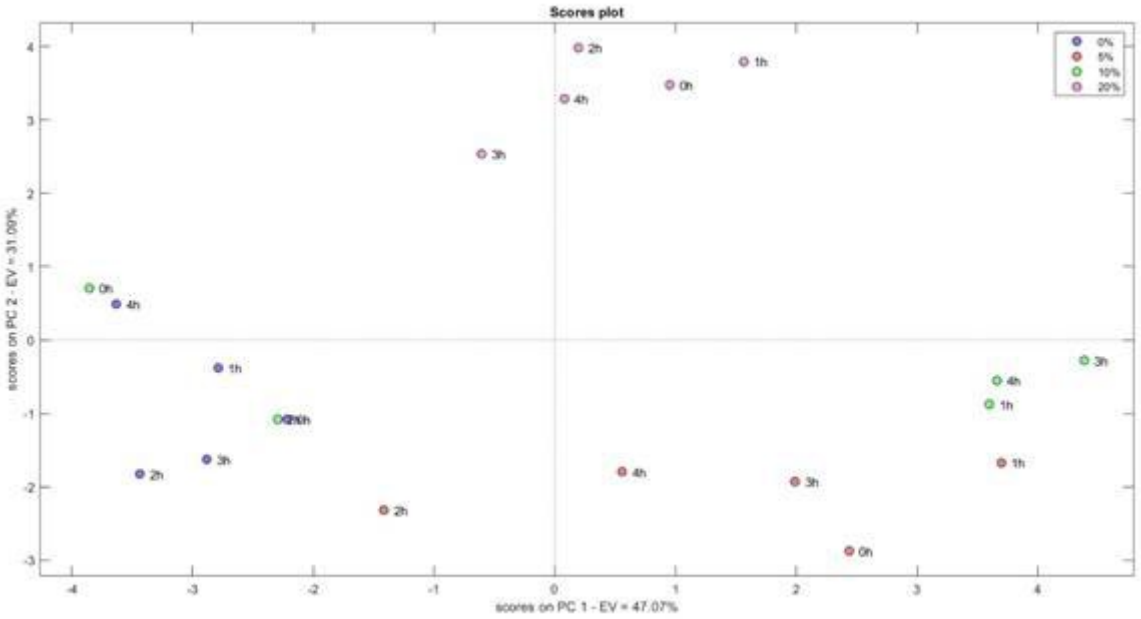

Figure S16. Scores plot for the PCA results from Raman.

Table S7. XRD PCA results.

component	eigenvalue	explained variance %	cumulative variance %
'PC1'	'302672211.8853'	'62.1084'	'62.1084'
'PC2'	'152427922.2212'	'31.2782'	'93.3866'
'PC3'	'11794807.507'	'2.4203'	'95.8069'

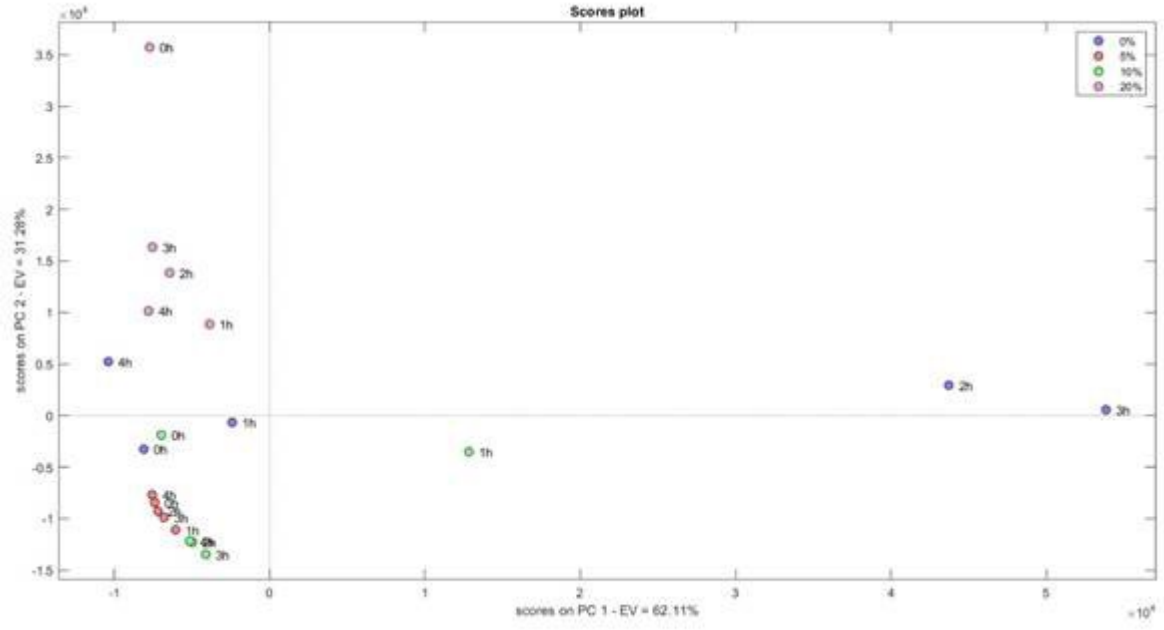

Figure S17. Scores plot for the PCA results from XRD.